MNRAS **000**, 1–10 (2018) Preprint 5 November 2019 Compiled using MNRAS LATEX style file v3.0

The first high-redshift Changing Look Quasars

Nicholas P. Ross[1]⋆, Matthew Graham[2], K. E. Saavik Ford[3,4,5], Barry McKernan[3,4,5] and Daniel Stern[6]

[1]*Institute for Astronomy, University of Edinburgh, Royal Observatory, Blackford Hill, Edinburgh EH9 3HJ, United Kingdom*
[2]*Cahill Center for Astronomy and Astrophysics, California Institute of Technology, Mail Code 249/17, 1200 E California Blvd, Pasadena CA 91125, USA*
[3]*Department of Science, BMCC, City University of New York, New York, NY 10007, USA*
[4]*Department of Astrophysics, Rose Center for Earth and Space, American Museum of Natural History, Central Park West at 79th Street, NY 10024, USA*
[5]*Graduate Center, City University of New York, 365 5th Avenue, New York, NY 10016, USA*
[6]*Jet Propulsion Laboratory, California Institute of Technology, 4800 Oak Grove Drive, Mail Stop 169-221, Pasadena, CA 91109, USA*

Accepted XXX. Received YYY; in original form ZZZ

ABSTRACT

We report on three redshift $z > 2$ quasars with dramatic changes in their C IV emission lines, the first 'Changing-Look" quasars at high redshift. This is also the first time the changing-look behaviour has been seen in a high-ionization emission line. SDSS J1205+3422, J1638+2827 and J2228+2201 show interesting behaviour in their observed optical light curves, and subsequent spectroscopy shows significant changes in the C IV broad emission line, with both line collapse and emergence being displayed in rest-frame timescales of ∼240-1640 days. Where observed, the profile of the Lyα/N V emission complex also changes, and there is tentative evidence for changes in the Mg II line. Although line measurements from the three quasars show large changes in the C IV line flux-line width plane, the quasars are not seen to be outliers when considered against the full $z \sim 2$ quasar population in terms of (rest) Equivalent Width and FWHM properties. We put these observations in context with recent "state-change" models, but note that even in their 'low-state', the C IV CLQs are above ∼10% in Eddington luminosity.

Key words: accretion, accretion discs – surveys – quasars: general – quasars: individual: J1100-0053

1 INTRODUCTION

Luminous AGN, i.e. quasars, are now seen to significantly vary their energy output on timescales of weeks to months. This observation, and the subsequent mismatch in the expected "viscous" timescale, which for a 10^7 $M_\odot$ central supermassive black hole (SMBH) is ∼hundreds of years, was noted over 30 years ago (e.g. Alloin et al. 1985). However, with new photometric light-curve and repeat spectroscopic data, the desire for a deeper understanding of AGN accretion disk physics has been recently re-invigorated the field (e.g. Lawrence 2018; Antonucci 2018).

The optical continuum variability of quasars has been recognized since their first optical identification (e.g., Matthews & Sandage 1963; MacLeod et al. 2012). Dramatic changes in the broad emission lines (BELs) of quasars has only recently been identified (e.g., LaMassa et al. 2015). Samples of over 100 "Changing Look" quasars (CLQs) or "Changing State" quasars (CSQs) have now been assembled (e.g. MacLeod et al. 2019; Graham et al. 2019). The community uses both these terms as a cover for the underlying physics. For sake of argument, "Changing Look" quasars can potentially be thought of as the extension to the BELs of quasar continuum variability (e.g., MacLeod et al. 2012) whereas the "Changing State" quasars (CSQs) have a 'state-transition' similar to that in Galactic X-ray binaries (Noda & Done 2018; Ruan et al. 2019). In this paper, we use the term 'Changing Look', as we are currently agnostic, and somewhat ignorant, to the underlying physical processes.

These CLQs have primarily been defined according to the (recombination) Balmer emission line properties with particular attention paid to the Hβ emission line, observed from optical spectroscopy. Recent work (Guo et al. 2019; Homan et al. 2019) report on discoveries of Mg II Changing-look AGN. However, current CLQ studies have been at redshifts $z < 1$.

While there have been a slew of studies on triply ionized carbon, i.e C IV, these have tended to focus on broad absorption line quasars (BAL QSOs; see Table 1 Hemler et al. 2019) or the Baldwin Effect (BEff; Baldwin 1977; Bian et al. 2012; Jensen et al. 2016; Hamann et al. 2017)[1]. Dramatic changes in the collisionally excited

⋆ E-mail: npross@roe.ac.uk

[1] As noted in Rakić et al. (2017), two different types of Baldwin effect are present in the literature: the *global* (or *ensemble*) Baldwin Effect, which is an anti-correlation between the EW of the emission line and the underlying continuum luminosity of *single-epoch* observations of a *large number* of

broad *emission* line (BEL) of C IV (and indeed C III]) have not to this point been seen.

Here, we report on three quasars which show dramatic changes in their C IV and C III] broad emission line properties as well as in the underlying continuum. We claim these are the first examples of "Changing Look Quasars" at high ($z > 1$) redshift. Moreover, these are the first cases for substantial changes of ions with high ionization potentials (I.P.'s >2 Rydberg), thus linking the ionizing photons to the energetic inner accretion disk, potentially by inverse Compton scattering of lower energy photons to higher energies. Furthermore, the measured rest-wavelengths of emission lines in quasar spectra, are known to vary from their nominal laboratory wavelengths especially for the high-ionization broad lines (e.g. Vanden Berk et al. 2001).

In this paper we use the wavelengths of 1548.202 and 1550.774 Å for the C IV doublet (Kramida et al. 2018). The 1548.202 and 1550.774 Å emission doublet is created by the $2p\ ^2P_0 - 2s\ ^2S$ transition, split by total angular momentum $J = 3/2$ and $1/2$, resulting in energies 64,591 cm^{-1} and 64,484 cm^{-1}, respectively (e.g. Moore 1993). The transition probabilities of the the 1548 and 1550Å lines are $A_{ki} = 2.65 \times 10^8$ and $2.64{\times}10^8$ s^{-1}.

The ground state of carbon is $1s^2\ 2s^2\ 2p^2$. Using the NIST Atomic Spectra Database Ionization Energies Form for ionisation energies, we note 11.3 eV is the energy required for C I to dislodge one electron and become singly-ionised C II; 24.4 eV is then the ('additional') energy needed for singly-ionised C II to dislodge an additional electron, and become doubly-ionised C III, and 47.89 eV (3.519 Ry) is required for doubly-ionised C III become triply-ionised C IV. 64.49 eV (4.74 Ry) is the energy needed to ionize C IV itself. This energy corresponds to a thermal temperature of $T \gtrsim 4{\times}10^5$, implying a heating energy source of (soft) X-ray photons ($k_B = 8.617{\times}10^{-5}$ eV /K). C III] is the $1s22s2p\ ^3\mathrm{P}^\circ$ to $1s^22s^2\ ^1\mathrm{S}$ transition (with $J = 1 \rightarrow 0$) resulting in an energy of 52,390.75 cm^{-1} and a transition probability of $A_{ki} = 1.14 \times 10^2$ s^{-1} (Wiese et al. 1996).

C IV variability has been long studied, e.g., Baldwin (1977); Gaskell (1982); Gregory et al. (1982); Wilkes (1986); Espey et al. (1989, 1990); Zheng & Sulentic (1990); Corbin (1990, 1991); Weymann et al. (1991); Dimitrijevic & Sahal-Brechot (1992); Tytler & Fan (1992); Wills et al. (1993); Brotherton et al. (1994); Osmer et al. (1994); Laor et al. (1995); McIntosh et al. (1999); Nazarova (2003).

Wilhite et al. (2006) examine the variability of a C IV sample of 105 quasars observed at multiple epochs by the Sloan Digital Sky Survey (SDSS; York et al. 2000; Stoughton et al. 2002; Abazajian et al. 2009a). They find a strong correlation between the change in the C IV line flux and the change in the line width, but no correlations between the change in flux and changes in line center and skewness. These authors find that the relation between line flux change and line width change is consistent with a model in which a broad line base varies with greater amplitude than the line core. The C IV lines in these high-luminosity quasars appear to be less responsive to continuum variations than those in lower luminosity AGN. Wilhite et al. (2006) find no evidence for variability of the well known blueshift of the C IV line with respect to the low-ionization Mg IIλ2798 line in the highest flux objects.

Richards et al. (2011) explored the BEL region in over 30,000 $z > 1.54$ SDSS quasars, concentrating on the properties of the C IV emission line. These authors consider two well-known effects involving the C IV emission line: *(i)* the anti-correlation between the C IV equivalent widths (EWs) and luminosity (i.e., the Baldwin Effect; BEff) and *(ii)* the blueshifting of the peak of C IV emission with respect to the systemic redshift. Richards et al. (2011) conclude that these two C IV parameters (EQW and blueshift) are capturing an important trade-off between "disk" and "wind" components in the disk-wind model of accretion disks (e.g., Murray et al. 1995; Elvis 2000; Proga et al. 2000), with one dominating over the other depending on the shape of the SED (Leighly 2004, strong C IV EQW indicates a more ionizing SED and large C IV blueshift indicating a less ionizing SED).

The Sloan Digital Sky Survey Reverberation Mapping Project (SDSS-RM; Shen et al. 2015) has a monitored ∼350 quasars with C IV. Noting the biases associated with C IV emission line properties (such as increasing systematic offsets with decreasing signal-to-noise; Denney et al. 2016), Grier et al. (2019) report report significant time delays between the continuum and the CIV 1549 emission line in 52 quasars, and investigate the C IV radius-luminosity relationship.

C IV is also known to exhibit significant displacements to the blue and these 'blueshifts' almost certainly signal the presence of strong outflows. As a consequence, single-epoch virial black hole (BH) mass estimates derived from C IV velocity widths are known to be systematically biased compared to masses from the hydrogen Balmer lines. Coatman et al. (2017) use a large sample of 230 high-luminosity ($L_{\mathrm{Bol}} = 10^{45.5-48}$ erg s^{-1}), redshift $1.5 < z < 4.0$ quasars with both C IV and Balmer line spectra, we have quantified the bias in C IVBH masses as a function of the C IV blueshift. C IV BH masses are shown to be a factor of 5 larger than the corresponding Balmer-line masses at C IV blueshifts of 3000 km s^{-1}1 and are overestimated by almost an order of magnitude at the most extreme blueshifts, ≳5000 km s^{-1}.

Sun et al. (2018) use the multi-epoch spectra of 362 quasars from the Sloan Digital Sky Survey Reverberation Mapping project to investigate the dependence of the blueshift of C IV relative to Mg II on quasar properties. We confirm that high-blueshift sources tend to have low C IV EWs, and that the low-EW sources span a range of blueshift. Other high-ionization lines, such as He II, also show similar blueshift properties. The ratio of the line width (measured as both the full width at half maximum and the velocity dispersion) of C IV to that of Mg II increases with blueshift. Quasar variability enhances the connection between the C IV blueshift and quasar properties (e.g., EW). The variability of the Mg II line center (i.e., the wavelength that bisects the cumulative line flux) increases with blueshift. In contrast, the C IV line center shows weaker variability at the extreme blueshifts. Quasars with the high-blueshift C IV lines tend to have less variable continuum emission, when controlling for EW, luminosity, and redshift. Our results support the scenario that high-blueshift sources tend to have large Eddington ratios. Therefore, according to this study, the C IV or [He II] EW is not an accurate indicator of the Eddington ratio or quasar SED. Recent investigations also include Meyer et al. (2019) and Doan et al. (2019). Dyer et al. (2019) provide a detailed analysis of 340 quasars at high-redshift ($1.62 < z < 3.30$) from the SDSS-RM project, which we will compare our results to.

The purpose of this paper is, for the first time, to access and report on the Changing-Look quasar phenomenon at high, $z > 2$ redshift. By doing so, we move from the low-ionization energy Balmer emission line series to the high-ionization emission lines, in particular C IV λ1549.

This paper is organised as follows. In Section 2, we describe our

AGN and second, the *intrinsic* Baldwin effect, the same anti-correlation but in an *individual, variable* AGN (Pogge & Peterson 1992).

Object R.A. / deg Decl. / deg	Redshift	g-band magnitude	MJD	Date	Instrument	Exposure Time / seconds	SDSS Spectrum Plate-FiberID	Notes
J120544.7+342252.4	2.068±0.0003	18.27	53498	2005-May-08	SDSS	8057	2089-427	
181.436164	2.071		58538	2019-Feb-24	DBSP	1800	—	Average conditions
+34.381229			58693	2019-Jul-29	DBSP	2400	—	
J163852.9+282707.7	2.185±0.0004	19.77	54553	2008-Mar-28	SDSS	4801	2948-614	
249.720558	2.186±0.0007		55832	2011-Sep-28	BOSS	3600	5201-178	
+28.452159	2.182		58583	2019-Apr-10	LRIS	1800	—	
J222818.7+220102.9	2.217±0.0021	19.97	56189	2012-Sep-19	BOSS	2700	6118-720	
337.078194	2.222±0.0004		56960	2014-Oct-30	BOSS	4500	7582-790	eBOSS reobservation
+22.017478			58693	2019-Jul-29	DBSP	2400	—	

Table 1. Details of our spectroscopic observations. Redshift and redshift errors from SDSS SkyServer for SDSS, BOSS and eBOSS spectra. Exposure times are from the `plate.fits` file. SDSS, BOSS and eBOSS spectra have $\mathcal{R}$ ∼2,000. DBSP: Double Spectrograph on the Palomar 200-inch telescope. LRIS: Low Resolution Imaging Spectrometer on Keck I 10m telescope.

sample selection, catalogs and observational data sets. In Section 3, we present the high-z quasars and report the line properties for the quasars at the observed epochs. We give a very brief theoretical discussion in Section 4. We present our Conclusions in Section 5. We report all magnitudes on the AB zero-point system (Oke & Gunn 1983; Fukugita et al. 1996) unless otherwise stated explicitly. For the WISE bands, $m_{\rm AB} = m_{\rm Vega} + m$ where $m = (2.699, 3.339)$ for WISE W1 at 3.4μm and WISE W2 at 4.6μm, respectively (Cutri et al. 2011). We adopt a flat ΛCDM cosmology with $\Omega_\Lambda = 0.73$, $\Omega_{\rm M} = 0.27$, and $h = 0.71$ in order to be consistent with Hamann et al. (2017). As a guide this cosmology has a $z = 2.000$ comoving radial distance of 5244.3 Mpc, a ∼1.25% difference compared to 5179.0 Mpc from $\Omega_\Lambda = 0.70$, $\Omega_{\rm M} = 0.30$, and $h = 0.70$ that is used in Shen et al. (2011).

2 DATA

Our high-z CLQs were identified as follows. We selected all 64,774 SDSS DR15 sources with $z > 0.35$ classified as 'QSO', having at least two spectra separated by at least 100 days, and with a corresponding CRTS light curve. We fitted a damped random walk to the CRTS data via Gaussian process regression and the photometric magnitudes at the epochs of the SDSS spectra for a given source are predicted. Those where $|\Delta V| > 0.3$ are then selected for visual inspection. Three quasars SDSS J120544.7+342252.4 (hereafter J1205+3422), SDSS J163852.93+282707.7 (hereafter J1638+2827) and SDSS J222818.76+220102.9 (hereafter J2228+2201), satisfied these selection criteria and showed interesting or dramatic emission line behaviour.

2.1 Spectra

An overview of our spectroscopic observations is given in Table 1. The spectra are from the SDSS (Stoughton et al. 2002; Abazajian et al. 2009b; Schneider et al. 2010), the SDSS-III Baryon Oscillation Spectroscopic Survey (BOSS Eisenstein et al. 2011; Dawson et al. 2013; Smee et al. 2013; Alam et al. 2015; Pâris et al. 2017) and the SDSS-IV Extended Baryon Oscillation Spectroscopic Survey (eBOSS; Dawson et al. 2016; Abolfathi et al. 2018; Pâris et al. 2018). These quasars were targetted via a range of techniques and algorithms (see Richards et al. 2002; Ross et al. 2012; Myers et al. 2015). The SDSS, BOSS and eBOSS data are supplemented by spectra from the Low Resolution Imaging Spectrometer (LRIS) on the 10m Keck I telescope (Oke et al. 1995). and the Double Spectrograph (DBSP) instrument on the Palomar *Hale* 5m telescope.

2.2 Emission Line and Power-law slope measurements

We use the measured quasar emission line properties from several catalogues: Shen et al. (2011), Hamann et al. (2017), Kozłowski (2017) and Calderone et al. (2017).

Shen et al. (2011) present a compilation of properties of the 105,783 quasars in the SDSS Data Release 7 (DR7) quasar catalog (DR7Q; Schneider et al. 2007). Shen et al. (2011) report non-zero C IV FWHM and EWs for approximately half (51,501) of the full DR7Q, and non-zero Mg II FWHM and EWs for 80% (84,183) of the DR7Q quasars). Measured line values using the methods and catalogue from Shen et al. (2011). $M_{\rm I}(z = 2)$ is the Absolute i-band magnitude K-corrected to $z = 2$; Bolometric luminosity computed from the monochromatic luminosity at 1350Å using the spectral fits and bolometric corrections (BC = 3.81) in Richards et al. (2006); Line luminosity, FWHM, rest-frame equivalent width, and their errors for the whole C IV profile. Power-law slope α_λ for the continuum fit for C IV; Virial BH masses using calibrations of Vestergaard & Peterson (2006). Eddington ratio computed using the virial BH mass.

Calderone et al. (2017) present the Quasar Spectral Fitting (QSFIT) software package which among other quantities provides luminosity estimates as well as width, velocity offset and equivalent width of 20 emission lines, including C IV, C III] and Mg II . We attempt to process and fit all nine spectra using the lastest version (v1.3.0) of the QSFIT online calculator and setting $E(B-V) = 0.00$. The host galaxy and blended iron emission at rest-frame optical wavelengths components are automatically disabled when they can not be constrained by the available data, such as the case for all our objects (we do not have infrared spectral data).

Hamann et al. (2017) investigate in robust detail the UV continuum and the C IV (and N V λ1238, 1242 Å) emission lines for over 200,000 quasars in BOSS DR12Q (Pâris et al. 2017). The quasar redshift are limited to the range $1.53 \leq z \leq 5.0$ so that C IV and the adjacent continuum are covered by BOSS. These measurements pro-

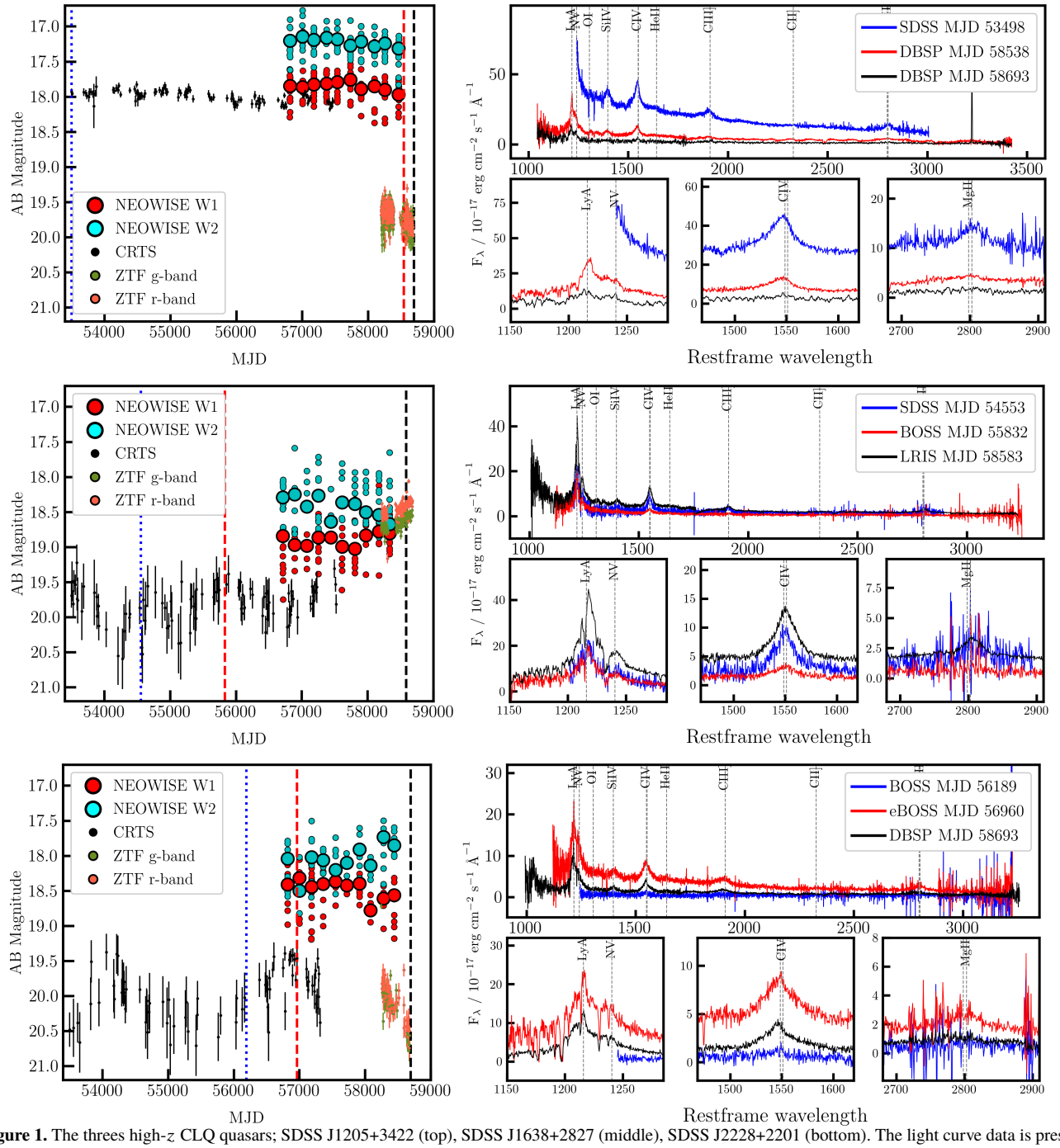

Figure 1. The threes high-z CLQ quasars; SDSS J1205+3422 (top), SDSS J1638+2827 (middle), SDSS J2228+2201 (bottom). The light curve data is present in the panels on the left hand side, with the spectral epoch observational timings given by the vertical lines. The spectra are on the right hand side, with zoom-in's on the Lyα-N v complex, the C iv line and the Mg ii line.

vide line profile information and flux ratios[2] Hamann et al. (2017) was focused on $z \geq 2$ quasars and specifcally their C ivproperties in order to understand the high-z "Extremely Red Quasar" population Ross et al. (2015); Zakamska et al. (2016); Perrotta et al. (2019); Zakamska et al. (2019). As such, we prefer the Hamann et al. (2017) emission line values where available, though this is only for two out of our nine spectra.

When using the Shen et al. (2011) catalogue, we report line luminosity, FWHM, rest-frame equivalent width, and their errors for the whole Mg ii profile (this catalogue also quotes values for just the broad Mg ii component, but the differences for our objects is negligible). The line luminosities in Calderone et al. (2017) are given in units of 10^{42} erg s^{-1}, while the line luminosities in Shen et al. (2011) are in units of $\log(L)$. We do not report the Shen et al. (2011) error on the line luminosity.

Power-law continuum slopes, α, where $f_\lambda \propto \lambda^\alpha$, are also reported in these catalogues and from QSFit. We quote the most appropriate value given the emission line wavelength.

[2] This emission-line catalog can be downloaded from here.

2.3 Multi-wavelength properties

Mid-infrared data (3.4 and 4.6μm) is available from the beginning of the Wide-field Infrared Survey Explorer (WISE) mission (2010 January; Wright et al. 2010) through the fifth-year of NEOWISE-R operations (2018 December; Mainzer et al. 2011). The WISE scan pattern leads to coverage of the full-sky approximately once every six months (a "sky pass"), but the satellite was placed in hibernation in 2011 February and then reactivated in 2013 October. Hence, our light curves have a cadence of 6 months with a 32 month sampling gap.

3 RESULTS

3.1 Overall Spectral Evolution

Figure 1 presents the optical and infrared light curves for three high-z CLQ quasars. Figure 1 also shows the spectra for each epoch, with the MJD of observation given by the dashed vertical lines in the light curves.

For J1205+3422, our spectral observations cover 5195 days observed, 1691 days in the rest-frame. For J1205+3422 is identified in SDSS as a bright $g \approx 18.0$, blue-sloped quasar with broad Si IV , C IV, C III] and Mg II observed in the initial spectrum (MJD 53498; 2005-May-08). C III] and C IV are seen to have large blueshifts of ≈2600±150 and ≈1150±100 km s^{-1}, respectively. By the time the 2019 spectra were taken (MJD 58538, 2019-Feb-24 and MJD 58693 2019-Jul-29), however, the light curve has dropped by ∼1.5 magnitudes and the spectra are significantly less steep. While Lyα and N V are detectable in both the MJD 58538 and MJD 58693 DBSP spectra, C IV has all but disappeared in the MJD 58693 spectrum. The broad C III] emission has disappeared between the 2005 and 2019 spectra. *The changes in C IV and C III] going from broad emission to barely detectable have on the timescales of ≈50 days in the rest-frame.*

For J1638+2827, our spectral observations cover 4030 days observed, 1265 days in the rest-frame. Here, in the initial epoch spectrum, C IV is broad and bright, as is C III] . However, just over 400 days in the rest-frame later, the broad C IV and C III] BEL have to faded, the continuum slope around 1400Å has changed from ≈-1.48 to ≈-2.25, but the Lyα /N V emission complex is very similar in shape and line flux intensity. Around 870 days in the rest-frame after the second spectral epoch, Lyα , N V , C IV, C III] and Mg II are all apparent and broad, with Mg II being seen for the first time at high signal-to-noise. The light curve is consistent with this spectral brightening, increasing from around ∼19.5-20.5th magnitude to ∼18.5 in the optical band. An absorption feature between Lyα and N V is seen in all three spectral epochs.

For J2228+2201, our spectral observations cover 2504 days observed, 778 days in the rest-frame. Over the course of 240 days in the rest-frame, C IV and C III] both *emerge* as BELs and the standard UV/blue continuum slope increases in flux. Then, over the course of 538 days in the rest-frame, the broadline emission, while still very present, reduces in line flux the UV/blue continuum diminishes, though is still more luminous than the initial BOSS spectrum.

3.2 Emission line evolution

Emission line measurements from the catalogues of Shen et al. (2011). Hamann et al. (2017), Kozłowski (2017) or the QSFit routine of Calderone et al. (2017) are presented in Table **??**.

From Figure 2 there appears to be a strong correlation between the change in the line flux and the change in the line width. Figure 2 shows the epoch-to-epoch flux ratio versus the ratio of line widths.

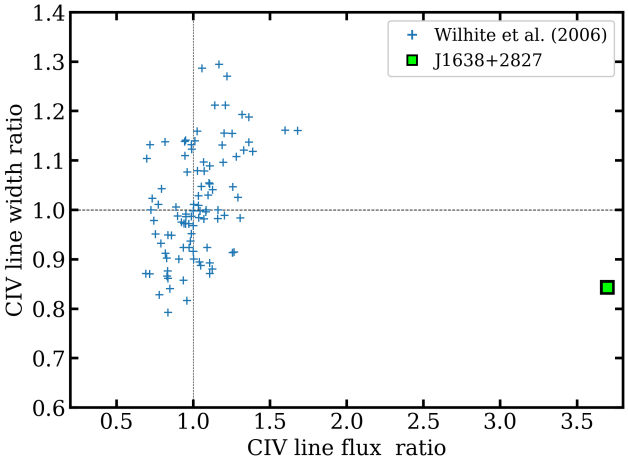

Figure 2. The Change in C IV line width vs. line flux change. We compare our object J1638+2827 with the sample from Wilhite et al. (2006) with a sample of 105 quasars observed at multiple epochs by the SDSS. J1638+2827 is a substantial outlier in this parameter space.

For the BOSS spectrum of J2228+2201 on MJD 56189, some of the data are "masked" (i.e. they have `and_mask` != 0) in the FITS file at wavelengths ≲1600Å (rest-frame). This typically means there is some potential problem in using those data. However, visual inspection shows strong broad C IV emission, so we disable the check on the mask, and report the line fits in Table **??**

3.3 The C IV Baldwin Effect

The Baldwin Effect (Baldwin 1977) is an empirical relation between emission-line REWs and continuum luminosity in quasars (Shields 2007; Hamann et al. 2017; Calderone et al. 2017) There is an anti-correlation between the emission-line REWs and e.g. 1450Å rest continuum luminosity, so that as the underlying UV continuum luminosity increases, the EW decreses, see Figure 4 Our Figure 4 is a reproduction of Figure 15 from Calderone et al. (2017).

The plotted values are `CONT1450\_\_LUM` and `BR\_CIV\_1549\_\_\EW`. `CONT1\_\_LUM` is the νL_ν luminosity at wavelength This selects 20,374 quasars.

The slope β is −0.1997. Checking with Kozłowski (2017), using their bolometric luminosity gives a slope of $\beta = -0.251$, in line with that from Hamann et al. (2017) ($\beta = -0.23$.

4 DISCUSSION

The variable properties of high-z quasars, however, has been less well studied. Reasons for this include more massive systems will tend to have longer timescales with e.g. $t_{\rm dyn} \sim M^2$ if $t_{\rm dyn} = \sqrt{R^3/GM}$ and $R_{\rm Sch} = 2GM/c^2$.

The Balmer series in hydrogen is due to the recombination cascade between different principal quantum numbers n, and the $n = 2$ level (e.g., Seaton 1959a,b). Lower redshift $z < 0.9$ CLQs have traditionally been identified via large changes in the Hβ emission line. Hβ emission is associated with a 2.55 eV energy difference. Thus we can place the high-z, HIL C IV in context of Balmer Hβ CLQs at lower-z.

C IV is one of the strongest collisionally excited lines in quasar

Object	MJD	line	Line Lumin.	FWHM	$V_{\rm off}$	E.W.	α_λ	Catalogue
	53498	C IV	511±13	9593±287	1172±74	15.9±0.4	−1.64 ± 0.01	QSFit
	53498	C IV	787	5230±219	1118±133	30.1±1.21	−1.47 ± 0.08	Shen2011
	53498	C IV	403	5119$^{(a)}$	—	—	—	DR12 SAS
	53498	C III]	441±10	14959±352$^{(b)}$	2616±147	25.10±0.59	−1.65 ± 0.01	QSFit
	53498	C III]	144	5119$^{(a)}$	—	—	—	DR12 SAS
	53498	Mg II	327±20	4907±387	−274 ± 419	26.66±1.65	−1.65 ± 0.01	$^{(d)}$QSFit
	53498	Mg II	284	4730±314	−179 ± 188	32±3.88	−1.87 ± 0.06	Shen2011
	53948	Mg II	130	5119$^{(a)}$	—	—	—	DR12 SAS
J1205+3422	58538	Lyα	952±1.1	12242±15	−1679 ± 6	165±0.2	—	QSFit
	58538	C IV	1037±5	>15000	983±40	—	—	QSFit
	58538	C III]	167±0.9	>15000	2734±46	45±0.2	—	QSFit
	58538	Mg II	216±1.4	13940±94	−465.2 ± 38	88±0.6	—	QSFit
	58693	Lyα	271±0.9	9637±52	−447 ± 13	85.1±0.3	—	QSFit
	58693	C IV	52±0.9	5046±26	1053±17	24.0±0.2	—	QSFit
	58693	C III]	59±0.9	10751±	1097±77	36±0.6	—	QSFit
	58693	Mg II	69±1.5	14983±346	−190 ± 134	72±1.6	—	QSFit
	54553	Lyα	188	3207	—	—	—	DR12 SAS
	54553	C IV	257±13	4550±371	55±450	31.8±1.5		$^{(d)}$QSFit
	54553	C IV	281	4181±736	680±133	100.5±12	−0.14 ± 0.68	Shen2011
	54553	C IV	170	4537$^{(a)}$	—	—	—	DR12 SAS
	54553	C III]	130±10	3852±402	−236 ± 565	36.7±2.8	−1.47 ± 0.20	$^{(d)}$QSFit
	54553	C III]	61	4537$^{(a)}$	—	—	—	DR12 SAS
	54553	Mg II	139	4757±2224	−944 ± 568	119±40	−1.49 ± 0.54	Shen2011
	54553	Mg II	69	4537$^{(a)}$	—	—	—	DR12 SAS
	55832	Lyα	288±11	4444±243	-463±68	103.69±3.99		QSFit
	55832	Lyα	234	4165.6$^{(a)}$	—	—	—	DR12 SAS
J1638+2827	55832	C IV	63±3	6052±250	-117±103	43.2±1.7	-2.25±0.05	QSFit
	55832	C IV	—	5210±226	—	42.8±2.0	−3.35	Ham17
	55832	C IV	46	5385$^{(a)}$	—	—	—	DR12 SAS
	55832	C III]	15±5	11421±3654	>3000	14.8±4.5	−2.25 ± 0.05	QSFit
	55832	C III]	11	5385$^{(a)}$	—	—	—	DR12 SAS
	55832	Mg II	13	5385$^{(a)}$	—	—	—	DR12 SAS
	58583	Lyα	785±1	4956±4	−641 ± 2	90±0.1	—	QSFit
	58583	C IV	311±1	5739±14	−167 ± 6	58±0.1	—	QSFit
	58583	C III]	52±0.8	3917.4 68.837	1514±127	124±2	—	QSFit
	58583	Mg II	157±2	10565±129	−450 ± 52	92±1	—	QSFit
	56189	C IV	32±3.5	7663±881	538±352	50.2±5.6	—	QSFit
	56189	C IV	—	2994±620	—	42.2±5.6	-1.59	Ham17
	56189	C IV	19	5218$^{(a)}$	—	—	—	DR12 SAS
	56189	C III]	34±6	13748±2869	1851±1140	63±12	−0.46 ± 0.21	QSFit
	56189	C III]	7	5218$^{(a)}$	—	—	—	DR12 SAS
	56189	Mg II	25±6	7253±1712	−931 ± 708	51±10.95	−0.46 ± 0.21	QSFit
	56189	Mg II	13	5218$^{(a)}$	—	—	—	DR12 SAS
	56960	Lyα	121±38	3580±673	-16±171	13.52 ±4.21	—	QSFit
J2228+2201	56960	C IV	229±4	8911±169	92±68	46.8±0.9	—	QSFit
	56960	C III]	185±5	-	2701±225	47.75±1.29	—	QSFit
	56960	Mg II	99±4	7312.6±340	188±137	50.75±2.21	—	QSFit
	58693	Lyα	447±5	8133±93	613±130	56±0.6	—	QSFit
	58693	C IV	41±1	4914± >65	160±27	25±0.3	—	QSFit
	58693	C III]	107±1.2	>15000	2422±67	—	—	QSFit
	58693	Mg II	177±1.1	>15000	1000±2617	16±36	—	QSFit

Table 2. Line Measurement information for the nine epochs for the 3 quasars. Line Luminosity is in units of 10^{42} erg s^{-1}; FWHM and $V_{\rm off}$ in km s^{-1}, where positive values of $V_{\rm off}$ means the line is blueshifted. Equivalent widths are ÅShen11 is Shen et al. (2011). Ham17 is Hamann et al. (2017). DR12 SAS is the line measurement information from the SDSS DR12 Science Archive Server (SAS). $^{(a)}$Emission lines of a common "width group", in this case, C IV1549, [He II] 1640, C III] 1909 and Mg II 2800 are constrained to have the same intrinsic velocity width in the SDSS spectral line fitting procedure (Bolton et al. 2012). Positive values of Voff means the line is blueshifted. Notes: QSFit does not fit the Mg II line for J1638+2827 MJD 54553 or 55832. QSFit does not fit the C IVline for J2228+2201 MJD 56189. $^{(d)}$Emission line modelled with two components. The different colours of text are merely for readability.

spectra Hamann & Ferland (e.g. 1999). The line is most prominent at n H ≈1010 cm−3 and log U≈-1.5, which are the canonical BELR parameters deduced over from early analysis of the C IV emission (Davidson & Netzer 1979). A dimensionless ionization parameter $U \equiv \Phi(H)/cn_H$, where c is the speed of light and n_H is the total hydrogen density ($H^0 + H^+$).

C IV probes the photoionization environment produced by the innermost disk, as indicated by RM time-delay measurements. In standard Shakura & Sunyaev (1973) thin disk models, large changes in the continuum flux are not permitted over short timescales due to the relatively long viscous time associated with such disks. Given the observed short timescale continuum variations, it is not surprising

Object	MJD	Cont. Lumin	Cont. slope
	53498	40040±34	-1.656± 0.006
J1205+3422	58538	—	—
	58693	—	—
	54553	3774±111	-1.472±0.197
J1638+2827	55832	2433±14	-2.316±0.051
	58583	3292±9	-0.541±0.010
	56189	—	—
J2228+2201	56960	7889±14	-1.729±0.015
	58693	—	—

Table 3. Quasar continuum νL_ν luminosities and slopes, at the fixed rest-frame wavelengths 1450Å from QSFIT. The luminosities are in units of 10^{42} erg s^{-1}.

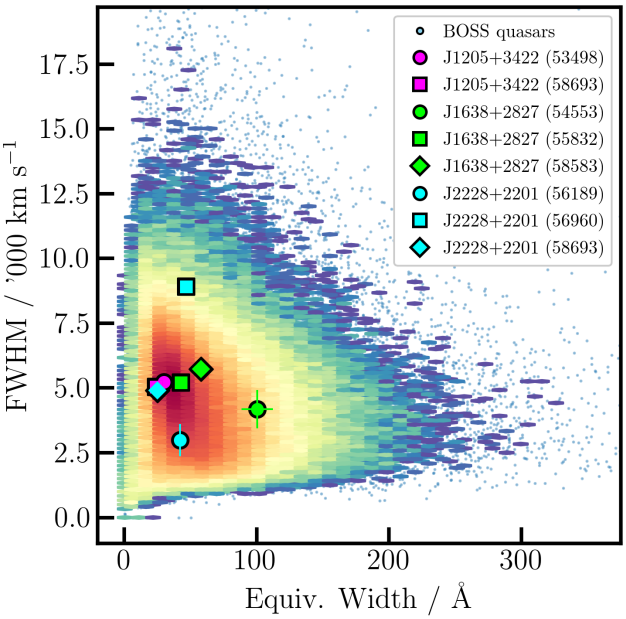

Figure 3. The Rest Equivalent Width (REW) vs. Full Width Half Maximum (FWHM) of the C IV emission line in the BOSS DR12 quasar sample using the catalogue of Hamann et al. (2017).

that the Shakura & Sunyaev (1973) disk may fail on other fronts. The C IV variations observed in our sources...

This indicates they may comfortably fit into the sample of CIV variable QSOs explored by Dyer et al. (2019), and similar to those authors we suggest slim accretion disk models e.g., Abramowicz et al. (1988) or inhomogeneous disk models (e.g., Dexter & Agol 2011) may provide viable explanations for our observations. I want to say a bit more here about the generic probe of photoionization vs shielding and conditions in the BL region but that will take more time.

This implies that the variable C IV in our sample arises through different emission mechanisms than is usual for high-z quasar...

4.1 The Baldwin Effect

The variable properties of the rest-frame UV quasar emission lines have been long studied, with the global (or ensemble) Baldwin Effect (the anti-correlation between the EW of the emission line and the underlying continuum luminosity of single-epoch observations of a

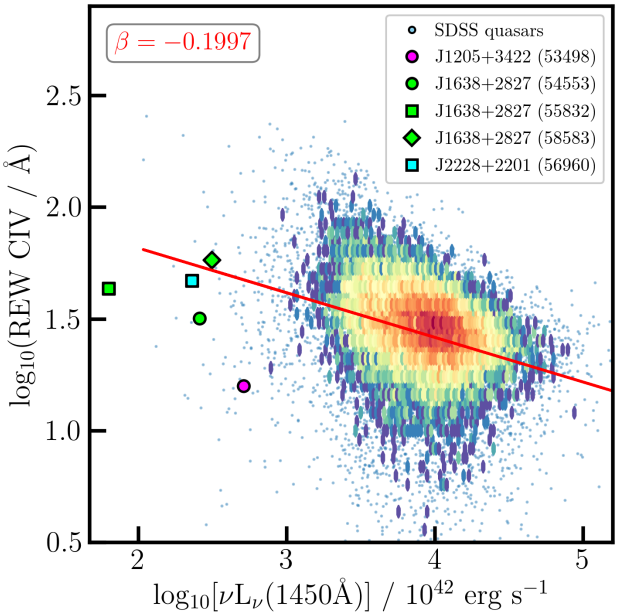

Figure 4. The C IV Equivalent width and the underlying continuum luminosity, commonly referred to as The Baldwin Plot. The continuum luminosities are from Kozłowski (2017), the REW measurements are Table 3.

large number of AGN, first noted in Baldwin (1977). More recently, the intrinsic Baldwin effect, the same anti-correlation but in an individual, variable AGN.

The X-ray Baldwin Effect (e.g., Iwasawa & Taniguchi 1993)... Bachev et al. (2004) find a 10-fold decrease in EW C IV with Eddington ratio (decreasing from ∼1 to ∼0.01), while N V shows no change. These trends suggest a luminosity-independent "Baldwin effect" in which the physical driver may be the Eddington ratio. Ge et al. (2016) Broad emission lines is a prominent property of type I quasi-stellar objects (QSOs).

4.2 Eddington ratios and State Changes

The broad UV and optical lines in quasars are most sensitive to the extreme ultraviolet (EUV) part of the spectral energy distribution (SED), with C IV (and indeed [He II] and N V) being at the higher energy end of the EUV distribution.

The soft X-ray excess – the excess of X-rays below 2 keV with respect to the extrapolation of the hard X-ray spectral continuum model – is a very common feature among type 1 active galactic nuclei (AGN). Noda & Done (2018) note that The soft X-ray excess produces most of the ionizing photons, so its dramatic drop leads to the disappearance of the broad-line region, driving the "changing-look" phenomena. major difference is that radiation pressure should be much more important in AGNs, so that the sound speed is much faster than expected from the gas temperature. This spectral hardening appears similar to the soft-to-hard state transition in black hole binaries at $L/L_{\rm Edd} \sim 0.02$ (i.e. $\eta_{\rm Edd} \sim -1.7$, where the inner disc evaporates into an advection dominated accretion flow, while the overall drop in luminosity appears consistent with the hydrogen ionization disc instability. Crucially Noda & Done (2018) make the prediction that all changing-look AGNs are similarly associated with the state transition at $L/L_{\rm Edd}$ ∼a few per cent. Jiang et al. (2014, 2016, 2019b). Jiang et al. (2019a) use global three dimensional radiation magneto-hydrodynamic simulations to study the properties

Object	MJD	M_i	$L_{\rm bol}$	$M_{\rm BH}$		$\eta_{\rm Edd}$		Ref.
				Mg II	C IV	Mg II	C IV	
J1205+3422	53498 58538 58693	-27.74	47.216±0.004	9.55±0.05	9.49±0.04	-0.434	-0.374	Shen11
J1638+2827	54553 55832 58583	-26.75 -26.40	46.166±0.04 46.721±0.073	9.03±0.37 9.34	8.74±0.15 9.13	-0.964 -0.717	-0.677 -0.509	Shen11 Kozl17
J2228+2201	56189 56960 58693	-25.46	46.231±0.073	9.45	8.73	-1.317	-0.602	Kozl17
M87*	57854	—	43.187	9.812±0.044		-4.699		EHT

Table 4. Physical properties of the C IV CLQs and M87. $M_I(z=2)$ is the Absolute i-band magnitude K-corrected to $z=2$; Bolometric luminosity computed from the monochromatic luminosity at 1350Å using the spectral fits and bolometric corrections (BC = 3.81) in Richards et al. (2006). Virial BH masses using calibrations of Vestergaard & Peterson (2006). $\eta_{\rm Edd}$ is the base 10 logarithm of the Eddington ratio computed using the virial BH mass. Shen11 is Shen et al. (2011). Kozl17 is Kozłowski (2017). EHT is Event Horizon Telescope Collaboration (2019e).

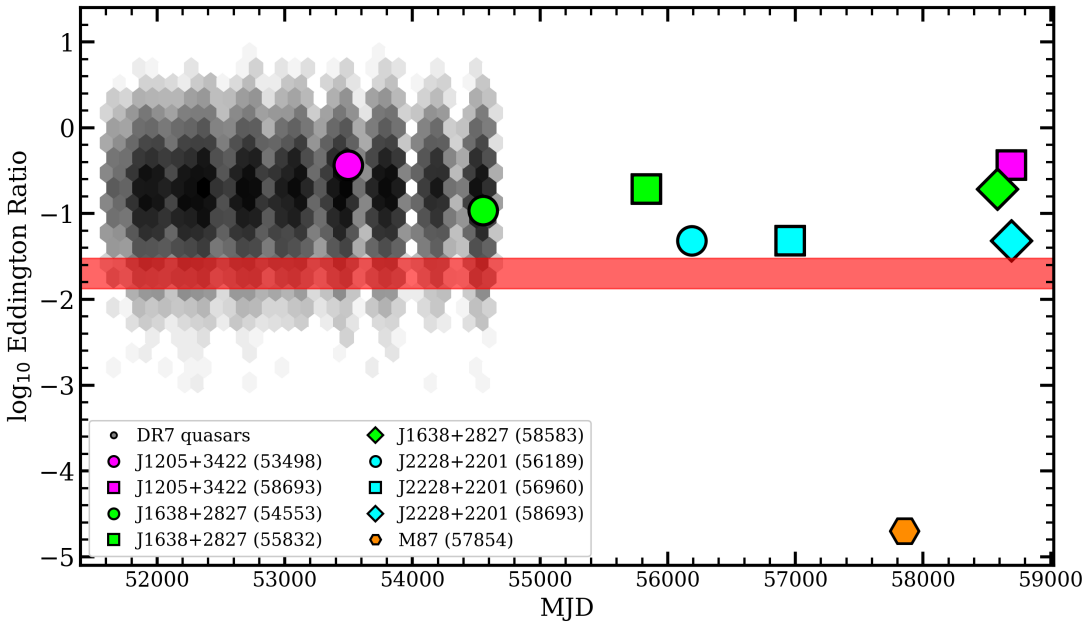

Figure 5. Eddington Ratios of the three C IV CLQs and M87.

of inner regions of accretion disks around a 5×10^8 $M_\odot$ black hole with mass accretion rates reaching 7% and 20% of the Eddington value.

We investigate this reporting the Eddington ratios of the three quasars in Table 4.

The Event Horizon Telescope (EHT) mapped the central compact radio source of the elliptical galaxy M87 at 1.3 mm (Event Horizon Telescope Collaboration 2019a,b,c,d,e,f) .

The EHT observsations confirm the observed 1.3mm asymmetric ring emission is consistent with predictions of strong gravitational lensing of synchrotron emission from a hot plasma orbiting near the black hole event horizon (Event Horizon Telescope Collaboration 2019e).

EHT2017 data includes tracks from four separate days of observing,;each day is $2.8 r_g\ c^{-1}$ (Event Horizon Telescope Collaboration 2019d) timescale is short compared to the decorrelation timescale of simulated images, which is ~50 $r_g\ c^{-1}$, and smaller than the light-crossing time of the source plasma.

From Event Horizon Telescope Collaboration (2019a), $M_{M87^*} = (6.5\pm0.7)\times10^9\ M_\odot$,

$$R_s = 2r_g = 2GM/c^2 = 9.598\times10^{12}\text{m}. \quad (1)$$

giving a *light crossing timescale* of $t_{\rm lt} = R_s/c$ = 32,015 secs (0.37 days).

$\log_{10}(M_{\rm M87^*}/M_\odot) = 9.813$. which is only about double that of J1205+3422 or J2228+2201, and a factor of ~6 that of J1638+2827. However, M87 has an Eddington accretion rate of $\approx140\ M_\odot\ {\rm yr}^{-1}$, and thus an Eddington ratio of $\dot{M}/\dot{M}_{\rm Edd} \sim 2\times10^{-5}$, i.e. $\eta_{\rm Edd} = -4.699$. (assuming the canonical accretion radiative efficiency of 10%; Di Matteo et al. 2003; Event Horizon Telescope Collaboration 2019e).

5 CONCLUSIONS

In this paper we have reported on three redshift $z>2$ quasars with dramatic changes in their C IV emission lines, the first 'Changing-

Look" quasars at high redshift. This is also the first time the changing-look behaviour has been seen in a high-ionization emission line.

- SDSS J1205+3422, J1638+2827 and J2228+2201 show interesting behaviour in their observed optical light curves, and subsequent spectroscopy shows significant changes in the C IV broad emission line, with both line collapse and emergence being displayed in rest-frame timescales of ∼240-1640 days.
- Where observed, the profile of the Lyα/N V emission complex also changes, and there is tentative evidence for changes in the Mg II line.
- Although line measurements from the three quasars show large changes in the C IV line flux-line width plane, the quasars are not seen to be outliers when considered against the full $z > 2$ quasar population in terms of (rest) Equivalent Width and FWHM properties.
- We put these observations in context with recent "state-change" models, but note that even in their 'low-state', the C IV CLQs are above ∼ 10% in Eddington luminosity.

Etiam mollis viverra nisi eget aliquet. Aliquam erat volutpat. Vivamus tristique, nisl eu malesuada semper, libero tortor convallis elit, a scelerisque orci nisi lacinia turpis. In lacinia ultrices volutpat. Proin ultrices luctus tellus, in placerat eros tincidunt id. Ut varius iaculis quam in consequat. Nulla nec orci est, sit amet Aliquam ac metus nec odio tempus pharetra sed nec diam. Sed eget arcu nulla. Etiam elementum ultrices ligula, at iaculis libero feugiat bibendum. Suspendisse potenti. Nam pharetra adipiscing euismod. Quisque imperdiet dignissim odio, sed volutpat justo tincidunt eu. Nunc vehicula pharetra suscipit. Integer aliquet pretium ipsum vel ultrices. Nam rutrum nibh ac quam pulvinar molestie.

Availability of Data and computer analysis codes

All materials, databases, data tables and code are fully available at: `https://github.com/d80b2t/CIV_CLQs`.

ACKNOWLEDGEMENTS

NPR acknowledges support from the STFC and the Ernest Rutherford Fellowship scheme.

We thank:

○ Dr. Giorgio Calderone for discussions to the utility of the QSFit routine and line measurements.
○ Andy Lawrence, Mike Hawkins and David Homan for useful discussion.

This paper heavily used TOPCAT (v4.4) (Taylor 2005, 2011). This research made use of `Astropy`, a community-developed core Python package for Astronomy (Astropy Collaboration et al. 2013; The Astropy Collaboration et al. 2018).

Funding for SDSS-III has been provided by the Alfred P. Sloan Foundation, the Participating Institutions, the National Science Foundation, and the U.S. Department of Energy Office of Science. The SDSS-III web site is http://www.sdss3.org/. SDSS-III is managed by the Astrophysical Research Consortium for the Participating Institutions of the SDSS-III Collaboration including the University of Arizona, the Brazilian Participation Group, Brookhaven National Laboratory, Carnegie Mellon University, University of Florida, the French Participation Group, the German Participation Group, Harvard University, the Instituto de Astrofisica de Canarias, the Michigan State/Notre Dame/JINA Participation Group, Johns Hopkins University, Lawrence Berkeley National Laboratory, Max Planck Institute for Astrophysics, Max Planck Institute for Extraterrestrial Physics, New Mexico State University, New York University, Ohio State University, Pennsylvania State University, University of Portsmouth, Princeton University, the Spanish Participation Group, University of Tokyo, University of Utah, Vanderbilt University, University of Virginia, University of Washington, and Yale University.

This publication makes use of data products from the Wide-field Infrared Survey Explorer, which is a joint project of the University of California, Los Angeles, and the Jet Propulsion Laboratory/California Institute of Technology, and NEOWISE, which is a project of the Jet Propulsion Laboratory/California Institute of Technology. WISE and NEOWISE are funded by the National Aeronautics and Space Administration. No animals were harmed in the production of this paper, but there was a large spider in NPRs apartment that "vanished".

REFERENCES

Abazajian K. N., et al., 2009a, ApJS, 182, 543
Abazajian K. N., et al., 2009b, ApJS, 182, 543
Abolfathi et al., 2018, ApJS, 235, 42
Abramowicz M. A., Czerny B., Lasota J. P., Szuszkiewicz E., 1988, ApJ, 332, 646
Alam S., et al., 2015, preprint, (arXiv:1501.00963)
Alloin D., Pelat D., Phillips M., Whittle M., 1985, ApJ, 288, 205
Antonucci R., 2018, Nature Astronomy, 2, 504
Astropy Collaboration et al., 2013, Astron. & Astrophys., 558, A33
Bachev R., Marziani P., Sulentic J. W., Zamanov R., Calvani M., Dultzin-Hacyan D., 2004, ApJ, 617, 171
Baldwin J. A., 1977, ApJ, 214, 679
Bian W.-H., Fang L.-L., Huang K.-L., Wang J.-M., 2012, MNRAS, 427, 2881
Bolton A. S., et al., 2012, AJ, 144, 144
Brotherton M. S., Wills B. J., Steidel C. C., Sargent W. L. W., 1994, ApJ, 423, 131
Calderone G., et al., 2017, MNRAS, 472, 4051
Coatman L., Hewett P. C., Banerji M., Richards G. T., Hennawi J. F., Prochaska J. X., 2017, MNRAS, 465, 2120
Corbin M. R., 1990, ApJ, 357, 346
Corbin M. R., 1991, ApJ Lett., 371, L51
Cutri R. M., et al., 2011, Technical report, Explanatory Supplement to the WISE Preliminary Data Release Products
Davidson K., Netzer H., 1979, Reviews of Modern Physics, 51, 715
Dawson K., et al., 2013, AJ, 145, 10
Dawson K. S., Kneib J.-P., et al., 2016, AJ, 151, 44
Denney K. D., et al., 2016, ApJS, 224, 14
Dexter J., Agol E., 2011, ApJ Lett., 727, L24
Di Matteo T., Allen S. W., Fabian A. C., Wilson A. S., Young A. J., 2003, ApJ, 582, 133
Dimitrijevic M. S., Sahal-Brechot S., 1992, A&AS, 96, 613
Doan A. N., et al., 2019, in American Astronomical Society Meeting Abstracts #233. p. 242.23
Dyer J. C., Dawson K. S., du Mas des Bourboux H., Vivek M., Bizyaev D., Oravetz A., Pan K., Schneider D. P., 2019, ApJ, 880, 78
Eisenstein D. J., Weinberg D. H., et al., 2011, AJ, 142, 72
Elvis M., 2000, ApJ, 545, 63
Espey B. R., Carswell R. F., Bailey J. A., Smith M. G., Ward M. J., 1989, ApJ, 342, 666
Espey B. R., Carswell R. F., Bailey J. A., Smith M. G., Ward M. J., 1990, ApJ, 354, 763
Event Horizon Telescope Collaboration 2019a, ApJ Lett., 875, L1
Event Horizon Telescope Collaboration 2019b, ApJ Lett., 875, L2

Event Horizon Telescope Collaboration 2019c, ApJ Lett., 875, L3
Event Horizon Telescope Collaboration 2019d, ApJ Lett., 875, L4
Event Horizon Telescope Collaboration 2019e, ApJ Lett., 875, L5
Event Horizon Telescope Collaboration 2019f, ApJ Lett., 875, L6
Fukugita M., Ichikawa T., Gunn J. E., Doi M., Shimasaku K., Schneider D. P., 1996, AJ, 111, 1748
Gaskell C. M., 1982, ApJ, 263, 79
Ge X., Bian W.-H., Jiang X.-L., Liu W.-S., Wang X.-F., 2016, MNRAS, 462, 966
Graham M. J., et al., 2019, arXiv e-prints, p. arXiv:1905.02262
Gregory S., Ptak R., Stoner R., 1982, ApJ, 261, 30
Grier C. J., et al., 2019, arXiv e-prints, p. arXiv:1904.03199
Guo H., Sun M., Liu X., Wang T., Kong M., Wang S., Sheng Z., He Z., 2019, ApJ Lett., 883, L44
Hamann F., Ferland G., 1999, ARA&A, 37, 487
Hamann F., et al., 2017, MNRAS, 464, 3431
Hemler Z. S., et al., 2019, ApJ, 872, 21
Homan D., Macleod C. L., Lawrence A., Ross N. P., Bruce A., 2019, arXiv e-prints, p. arXiv:1910.11364
Iwasawa K., Taniguchi Y., 1993, ApJ Lett., 413, L15
Jensen T. W., et al., 2016, ApJ, 833, 199
Jiang Y.-F., Stone J. M., Davis S. W., 2014, ApJ, 796, 106
Jiang Y.-F., Davis S. W., Stone J. M., 2016, ApJ, 827, 10
Jiang Y.-F., Blaes O., Stone J., Davis S. W., 2019a, arXiv e-prints, p. arXiv:1904.01674v1
Jiang Y.-F., Stone J. M., Davis S. W., 2019b, ApJ, 880, 67
Kozłowski S., 2017, ApJS, 228, 9
Kramida A., Ralchenko Y., Reader J., NIST ASD Team 2018, doi:10.18434/T4W30F,
LaMassa S. M., et al., 2015, ApJ, 800, 144
Laor A., Bahcall J. N., Jannuzi B. T., Schneider D. P., Green R. F., 1995, ApJS, 99, 1
Lawrence A., 2018, Nature Astronomy, 2, 102
Leighly K. M., 2004, ApJ, 611, 125
MacLeod C. L., et al., 2012, ApJ, 753, 106
MacLeod C. L., et al., 2019, ApJ, 874, 8
Mainzer A., et al., 2011, ApJ, 731, 53
Matthews T. A., Sandage A. R., 1963, ApJ, 138, 30
McIntosh D. H., Rix H. W., Rieke M. J., Foltz C. B., 1999, ApJ Lett., 517, L73
Meyer R. A., Bosman S. E. I., Ellis R. S., 2019, arXiv e-prints,
Moore C. E., 1993, Tables of Spectra of Hydrogen, Carbon, Nitrogen, and Oxygen Atoms and Ions
Murray N., Chiang J., Grossman S. A., Voit G. M., 1995, ApJ, 451, 498
Myers A. D., et al., 2015, ApJS, 221, 27
Nazarova L. S., 2003, Astronomical and Astrophysical Transactions, 22, 681
Noda H., Done C., 2018, MNRAS, 480, 3898
Oke J. B., Gunn J. E., 1983, ApJ, 266, 713
Oke J. B., et al., 1995, PASP, 107, 375
Osmer P. S., Porter A. C., Green R. F., 1994, ApJ, 436, 678
Pâris I., Petitjean P., Ross N. P., et al., 2017, Astron. & Astrophys., 597, A79
Pâris I., et al., 2018, Astron. & Astrophys.
Perrotta S., Hamann F., Zakamska N. L., Alexand roff R. M., Rupke D., Wylezalek D., 2019, MNRAS, 488, 4126
Pogge R. W., Peterson B. M., 1992, AJ, 103, 1084
Proga D., Stone J. M., Kallman T. R., 2000, ApJ, 543, 686
Rakić N., La Mura G., Ilić D., Shapovalova A. I., Kollatschny W., Rafanelli P., Popović L. Č., 2017, Astron. & Astrophys., 603, A49
Richards G. T., et al., 2002, AJ, 123, 2945
Richards G. T., et al., 2006, ApJS, 166, 470
Richards G. T., et al., 2011, AJ, 141, 167
Ross N. P., et al., 2012, ApJS, 199, 3
Ross N. P., et al., 2015, MNRAS, 453, 3932
Ruan J. J., Anderson S. F., Eracleous M., Green P. J., Haggard D., MacLeod C. L., Runnoe J. C., Sobolewska M. A., 2019, arXiv e-prints, p. arXiv:1903.02553v1
Schneider D. P., et al., 2007, AJ, 134, 102
Schneider D. P., et al., 2010, AJ, 139, 2360
Seaton M. J., 1959a, MNRAS, 119, 81
Seaton M. J., 1959b, MNRAS, 119, 90
Shakura N. I., Sunyaev R. A., 1973, Astron. & Astrophys., 24, 337
Shen Y., et al., 2011, ApJS, 194, 45
Shen Y., et al., 2015, ApJS, 216, 4
Shields J. C., 2007, in Ho L. C., Wang J. W., eds, Astronomical Society of the Pacific Conference Series Vol. 373, The Central Engine of Active Galactic Nuclei. p. 355 (arXiv:astro-ph/0612613)
Smee S. A., et al., 2013, AJ, 146, 32
Stoughton C., et al., 2002, AJ, 123, 485
Sun M., Xue Y., Richards G. T., Trump J. R., Shen Y., Brandt W. N., Schneider D. P., 2018, ApJ, 854, 128
Taylor M. B., 2005, in Shopbell P., Britton M., Ebert R., eds, Astronomical Society of the Pacific Conference Series Vol. 347, Astronomical Data Analysis Software and Systems XIV. p. 29
Taylor M., 2011, TOPCAT: Tool for OPerations on Catalogues And Tables, Astrophysics Source Code Library (ascl:1101.010)
The Astropy Collaboration et al., 2018, preprint, (arXiv:1801.02634v2)
Tytler D., Fan X.-M., 1992, ApJS, 79, 1
Vanden Berk D. E., et al., 2001, AJ, 122, 549
Vestergaard M., Peterson B. M., 2006, ApJ, 641, 689
Weymann R. J., Morris S. L., Foltz C. B., Hewett P. C., 1991, ApJ, 373, 23
Wiese W. L., Fuhr J. R., Deters T. M., 1996, Journal of Physical and Chemical Reference Data, 532
Wilhite B. C., Vanden Berk D. E., Brunner R. J., Brinkmann J. V., 2006, ApJ, 641, 78
Wilkes B. J., 1986, MNRAS, 218, 331
Wills B. J., Brotherton M. S., Fang D., Steidel C. C., Sargent W. L. W., 1993, ApJ, 415, 563
Wright E. L., et al., 2010, AJ, 140, 1868
York D. G., et al., 2000, AJ, 120, 1579
Zakamska N. L., et al., 2016, MNRAS, 459, 3144
Zakamska N. L., et al., 2019, MNRAS, 489, 497
Zheng W., Sulentic J. W., 1990, ApJ, 350, 512

This paper has been typeset from a TEX/LATEX file prepared by the author.